Behavior of Mg–Si-Rich Phases in Aluminum Can Sheets and Their Impact on Metal Oxidation During Industrial Thermal Pre-treatment

Article · February 2018

DOI: 10.1007/978-3-319-72284-9_146

CITATIONS
2

READS
27

4 authors, including:

Jan Steglich
TRIMET Aluminium SE
11 PUBLICATIONS **6** CITATIONS
SEE PROFILE

Bernd Friedrich
RWTH Aachen University
700 PUBLICATIONS **2,852** CITATIONS
SEE PROFILE

Behavior of Mg–Si-Rich Phases in Aluminum Can Sheets and Their Impact on Metal Oxidation During Industrial Thermal Pre-treatment

J. Steglich, C. Matthies, M. Rosefort, and B. Friedrich

Abstract

Aluminum beverage can (UBC) recycling is a combined process of de-coating and submerged melting. The de-coating temperature varies in industrial processes and is often chosen higher than required for coating removal in order to maximize metal production. Isothermal annealing experiments with EN AW-5182 and EN AW-3104 can sheets were performed to investigate the influence of Mg–Si-rich phases on oxidation mechanism during pre-treatment. A discrete change from diffusion to liquid metal transport is observed after which extensive oxidation starts immediately. Scanning electron microscope with energy-dispersive X-ray spectroscopy (SEM EDX) analysis was used to trace the transport mechanisms starting at solid Mg–Si-phases. The transport mechanism was verified with thermochemical calculations. A maximum pre-treatment temperature of 843 K (1058 °F) is derived, reducing the process temperature range to 823–843 K. Finally, the results were transferred to industrial UBC remelting processes to minimize metal losses.

Keywords

Mg–Si diffusion • Oxidation behavior • Aluminum beverage can recycling

Introduction

Used beverage can scrap (UBC) is always contaminated with organic coating and often contains additional organic impurities as beverage residues and plastics. UBC has to be thermally de-coated to remove the organics, as the impurities lead to dross formation and their residues contaminate the melt in a recycling furnace [1]. The industrial de-coating is performed either in a separated rotary kiln (de-coater) or in a combined multi chamber furnace. The de-coating temperature varies widely within a range of 723–873 K in rotary kilns [2] and 873–1023 K in multi chamber furnaces [3]. Although a temperature of 823 K is sufficient to remove the coating [1], the temperature is often chosen higher to speed up the heat transfer into the scrap and reduce treatment time. Because oxygen is necessary for successful de-coating [1], metal oxidation has to be limited simultaneously during thermal pre-treatment.

UBC recycling experiments by [4] quantify the impact of oxidation for one scrap type during the thermal pre-treatment and subsequent melting. UBC bales with a density of 910 kg/m^3 were de-coated in a 65 t industrial multi-chamber furnace with pre-heating shaft. A charge of about 100 kg UBC bales was equipped with thermocouples and placed in the pre-heating shaft without direct contact to the melt. The pre-heating shaft had a temperature of 873–933 K without the combustion of organics under regular production conditions. A heating rate between 10 and 14 K/min was recorded in the center of the bales, depending on the location of the bales in the charge. As a result, the bales reached a target de-coating temperature of 823 K within 40–55 min in the center. By this time, major parts of the bale were already oxidized by exceeding the target temperature. Subsequent re-melting experiments without salt flux showed, that the oxidized bales produced about 25% more dross and 2% more metal loss than not oxidized samples of the same scrap charge, in laboratory scale. The following study shows that the can end sheets oxidize within minutes, if the temperature of the metal exceeds 843 K.

J. Steglich (✉) · C. Matthies · M. Rosefort
TRIMET Aluminium SE, Aluminiumallee 1, 45356 Essen, Germany
e-mail: jan.steglich@trimet.de

B. Friedrich
IME Process Metallurgy and Metal Recycling, RWTH Aachen University, Intzestr. 3, 52056 Aachen, Germany

O. Martin (ed.), *Light Metals 2018*, The Minerals, Metals & Materials Series,
https://doi.org/10.1007/978-3-319-72284-9_146

Literature Survey on Can Alloy Oxidation During Thermal Pre-treatment

The oxidation rate of an EN AW-5182 can end alloy was investigated by [5] with thermogravimetric analysis (TGA) at different temperatures. The metal oxidation rate of an alloy can be expressed as its weight gain over time, measured by TGA. The oxidation up to 20 h at 823 K leads to minimal weight gain, whereas the oxidation rate triples at 923 K in the semi solid state and increases linear over time. The experiments were repeated with alloys containing 1 wt % Mg (EN AW-3004, former can body alloy) and no magnesium. It is known that a rising Mg concentration increases the oxidation rate of the alloy drastically. On liquid melts, it was concluded that the rupturing of the protective oxide surface leads to direct oxidation of molten metal and resulted in growth of secondary oxide nodules [5]. In liquid state, this mechanism is referred to as breakaway-oxidation in the literature [3, 5, 11].

A similar mechanism is described by [6] for solid state oxidation. Isothermal annealing experiments with AlMg5 sheets were performed in dry air at 823 K up to 90 h. After 45 h, local detachments of the surface MgO layer on the sheet were observed. These detachments were caused by voids at the metal-oxide interface, created by outward diffusion of Mg through the oxide layer. SEM analysis show that these voids started to grow near to the grain boundaries. Growing oxide nodules cause cracks in the oxide layer and lead to none-protective metal oxidation. Continuous oxidation over 90 h resulted in extensive MgO formation on the sheet surface having a "*Cauliflower*" [6] like morphology. The formation of a similar morphology was also observed on AlMg4 sheets during isothermal melting at 1023 K in dry air by [7]. After 5 min, MgO started to develop on the molten sheet, which was analyzed by SEM EDX. It shows the formation of Al_2MgO_4 beneath the MgO at the metal-oxide interface during oxidation. After 3 h, nodular oxide growth was microscopically visible on the sheet containing Al_2MgO_4, MgO and Al_2O_3 [7]. The time until none-protective metal oxidation occurred was up to 90 h in the solid state [6] and up to 3 h in the liquid state [7].

The TGA of [8] and [9] compare the oxidation rate of pure aluminum and an AlMg alloy within relevant time and temperature for thermal pre-treatment. The oxidation rate of aluminum sheet with 4.2 wt% Mg was investigated by [9] and is plotted over time in Fig. 1 for different temperatures. A significant increase of the oxidation rate is shown by a rise of temperature from 793 K (968 °F) to 848 K (1067 °F). These results are compared to investigations by [8] on the oxidation rates of pure aluminum. The oxidation rate of AlMg4.2 sheet is about 50 times higher than of pure Al sheets at a temperature range between 843 and 848 K, as shown in Fig. 1. It is therefore expected that the magnesium rich can end sheets oxidize significantly during an estimated pre-treatment time of 20–50 min and a process temperature of 848 K.

For binary aluminum alloys it is generally accepted that liquid state oxidation is increased by Mg, Na and Ca while the elements Mn, Fe, Cu and Si show no or little effect on oxidation [3, 10]. However, the interaction of these elements in a multicomponent system is not fully understood. The present experiments show that Si serves as a possible oxidation trigger in a ternary Al–Mg–Si system in none-equilibrium state. The influence of Si on the oxidation of an AlMg alloy was studied by [11]. The oxidation rate of an AlMg3 melt was measured at 1383 K in dry air by TGA. SEM EDX analysis of solidified metal samples were carried out to investigate oxide morphology and composition. As a result of the measurements, a parabolic oxidation rate is shown up to 30 h of oxidation time, followed by a linear increase up to 80 wt% of the sample weight in additional 15 h. In an additional experiment, 7 wt% Si were added to the initial AlMg3 alloy. This time, the linear oxidation rate started after 5 h and reached the same weight gain as the previous sample after only 15 h. The drastic reduction of incubation time was explained by a lower viscosity of the Si rich melt. The Si-rich metal penetrates easier into cracks and pores of the MgO/Al_2MgO_4 oxide layer, leading to an early start of none-protective oxidation [11].

The literature review shows that the oxidation rate of solid AlMg4.2 sheets increases drastically when the temperature is raised from 793 to 848 K. It is also shown that Si reduces the incubation time until linear oxidation starts on an Al–Mg–Si melt. In the present study, it is investigated, if Mg–Si-rich phases are responsible for the discrete change from solid state oxidation to liquid metal oxidation within minutes. It is also the aim to describe the temperature at

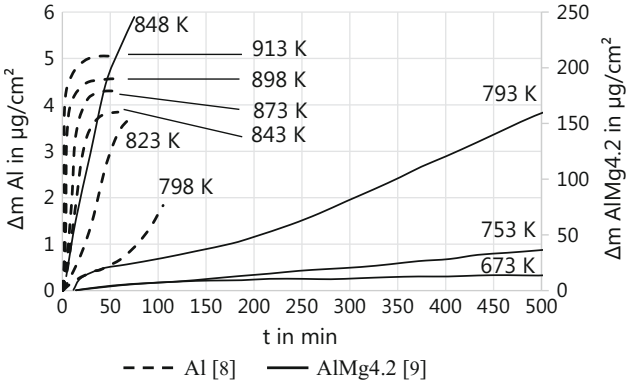

Fig. 1 TGA showing the weight gain (Δm) by oxidation of pure aluminum (Al) and aluminum magnesium (AlMg4.2) sheets in dry oxygen according to [8, 9]

which the oxidation kinetics change to formulate a maximum thermal pre-treatment temperature for beverage can sheets.

Experiment Procedure

EN AW-3104 and EN AW-5182 can sheets with a thickness of 230 and 270 µm were used respectively. The element composition of the EN AW-3104 sheet was analyzed by ICP OES, while the EN AW-5182 sheet was analyzed by spark optical emission spectroscopy, depending on the acceptable sample thickness for the method. The results are given in Table 1.

The sheets were cut into pieces of 31 × 31 mm, cleaned with acetone and afterwards washed with demineralized water. The pieces were placed on a refractory board and annealed isothermally in an air convection furnace. Table 2 shows the according annealing temperatures and times. In each experiment, the effective sheet temperature was measured with a reference sample, which was equipped with a thermocouple type K. During sampling, the sheet temperatures remained constant within a range of 2–3 K.

After the annealing time, one sample of each sheet was taken out of the furnace, cooled rapidly on a steel plate and mounted in a two component embedding resin. After metallographic investigation, the samples were analyzed by SEM EDX. A reference sample of the two sheets was analyzed as well.

Results and Discussion

Thermochemical equilibrium calculations of the two alloy systems EN AW-3104 and EN AW-5182 are used to describe the dissolution of intermetallic phases into the aluminium matrix. The results are shown in Figs. 2 and 3. The phase diagrams are calculated with the software Pandat Version 2017 using the database PanAl2017 [12]. The Mg concentration is shown on the X-axis and the measured magnesium concentration is marked as dotted line in both phase diagrams. The phases are labeled in decreasing order of composition in the diagrams.

In the EN AW-3104 phase diagram, primary α-aluminum and intermetallic Al_6FeMn, $Al_{15}FeMn_3Si_2$ and Mg_2Si phases are stable at 673 K. With increasing temperature, the system has a large stability region for α-aluminum and $Al_{15}FeMn_3Si_2$.

If the temperature exceeds ca. 900 K, the first liquid phase (L) is formed, but the $Al_{15}FeMn_3Si_2$ phases remain stable. Only 30 K higher, the alloy is completely liquid.

The phase diagram of the EN AW-5182 alloy (Fig. 3) shows a wide stability region of α-aluminum with $Al_{15}FeMn_3Si_2$ and Mg_2Si phases up to 823 K at the measured Mg concentration. When this temperature is exceeded, the Mg_2Si-phases should dissolve in surrounding matrix. At 843 K, the first liquid phase (L) is formed, which is rich in Mg and Si as they are the first dissolving phases. An $Al_{13}Fe_4$-phase is formed, which is described as an AlCu-phase with Fe, Mn and Zn as well as Si and Zn substitutions in the PanAl2017 database [12].

The phase diagram of the EN AW-5182 alloy shows no liquid phases at 793 K. However at 823 K, the Mg_2Si--phases are dissolved and form the first liquid phase at 843 K already. The beginning formation of a liquid phase above 843 K could be the reason for the drastic change in oxidation behavior of a similar AlMg4.2 alloy, presented above in Fig. 1.

(a) Light microscopic observations

The impact of phase transformation from solid to solute enriched liquid in the can sheets are compared via optical microscope investigations, see Figs. 4 and 5. All photos are taken as transverse cross sections to the grain orientation from the sheets. The top surface of the samples was exposed to the furnace atmosphere, while the bottom surface was laying on the refractory board. No visible change of both sheet surfaces can be detected even after 5 h oxidation at 823 K in air (Fig. 4). Only the visible density of

Table 1 Element analysis of EN AW-3104 can body and EN AW-5182 can end sheet

Element in wt%	Mg	Mn	Cu	Si	Fe	Cr	Zn	Ti	Al
EN AW-3104	1.30	0.98	0.17	0.29	0.47	0.02	<0.01	0.02	Rest
SD	0.01	0.01	0	0	0	0	0	0	–
EN AW-5182	4.41	0.29	0.02	0.15	0.23	0.02	<0.01	0.01	Rest
SD	0.001	0.001	0	0.001	0.003	0	0	0	–

Table 2 T-t-Parameters of isothermal annealing experiments

Experiment	Annealing time in min
823 ± 2 K (1022 ± 2 °F)	60, 120, 180, 240, 320
873 ± 2 K (1112 ± 2 °F)	7, 10, 14, 21, 28, 35, 42, 49, 56

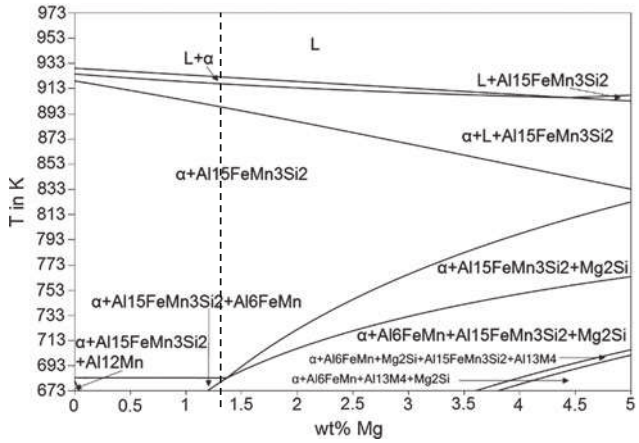

Fig. 2 Phase diagram of the EN AW-3104 alloy with variable magnesium content, calculated using the software Pandat Version 2017 [12]

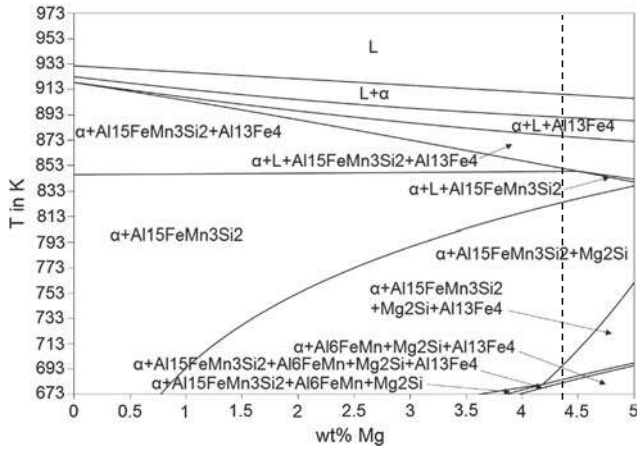

Fig. 3 Phase diagram of the EN AW-5182 alloy with variable magnesium content, calculated using the software Pandat Version 2017 [12]

intermetallic phases in both sheets has decreased. Molten areas did not form, as expected from the phase diagrams.

On the other hand, Fig. 5 shows no change of the EN AW-3104 sheet surface, but a significant change in structure of the EN AW-5182 sheet after annealing at 873 K. Between 7 and 10 min, voids are formed along grain boundaries, revealing their oval shape, indicated with (1) in Fig. 5. Due to micro-segregation, the grain boundaries are richer in solute than the α-aluminum phases that have grown in the grain [13]. According to Fig. 3, Mg_2Si-phases dissolve and form a liquid Phase at 873 K, but not at 823 K. The liquid phase formation leads to volume expansion due to the lower density of the liquid. The overpressure is compensated by pushing the top grains out of the sheet surface (2). Finally, the Mg–Si-rich melt oxidizes directly in the furnace atmosphere and continuous to form the "*Cauliflower*" [6] within 21–56 min,

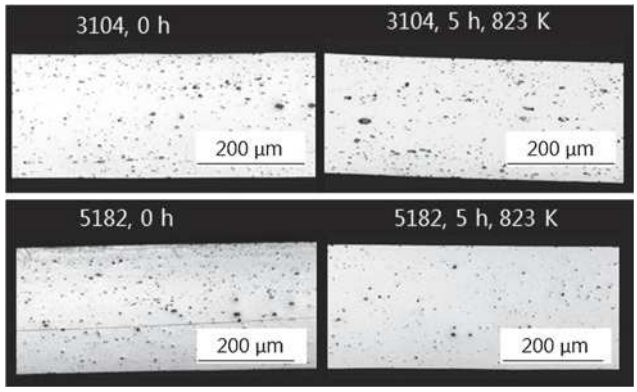

Fig. 4 Optical microscope polished cross sections of the EN AW-3104 and EN AW-5182 can sheets after isothermal annealing at 873 K and given time

indicated with (3). The change in composition of the dissolving phases and metal oxides will be confirmed with the results of SEM EDX analysis.

(b) SEM EDX phase analytics (Detection of Mg–Si-rich phases)

In the Al–Mg–Si system, the MgSi-phase has an approximate composition of Mg_2Si [14]. In the aluminum-rich corner, there are two ternary invariant reactions with the two subsystems α-Mg_2Si–Si and α-β-Mg_2Si. The β-phase equals Al_8Mg_5 [16]. The two subsystems are commonly found in industrial alloys and are described by [14]:

- L1 ↔ α+Si+Mg_2Si with 4.9% Mg and 14.6% Si at 831 K
- L2 ↔ α+Mg_2Si+ β with 33.9% Mg and 0.07% Si at 721 K

In the initial sheet sample (0 min) of EN AW-5182, AlFe (Mn, Si) and MgSi-phases are detected in the matrix by SEM EDX with an acceleration voltage of EHT = 12 kV, shown in Fig. 6 (left). Comparing to the sample after isothermal heating at 873 K for 10 min in Fig. 6 (right), phase transformation is clear visible. The heat treated sample contains microstructure zones similar to L1 and L2, defined here as L1′ and L2′. Latter L2′ consists of about 27 wt% Mg and almost no Si, L1′ is composed of approximately 2 wt% Mg and 27 wt% Si. It is assumed, that more Si will dissolve in L2′ with longer annealing time to approach composition of L2. It is concluded that thermal pre-treatment of can end sheets at 873 K leads to the formation of a Mg- and Si-enriched liquid phase L in none-equilibrium state, which oxidizes easily in contact with the furnace atmosphere.

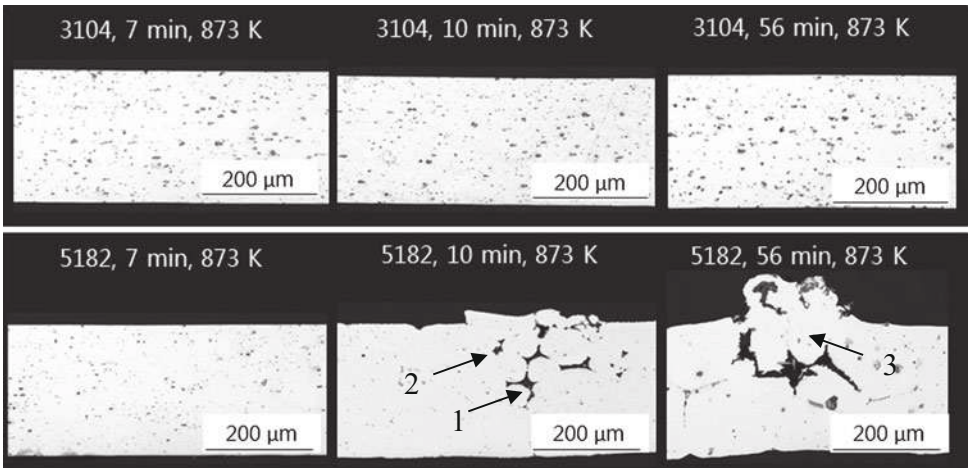

Fig. 5 Optical microscope polished cross sections of the EN AW-3104 and EN AW-5182 can sheets after isothermal annealing at 873 K and given time

(c) SEM EDX surface analytics (Liquid metal transport and oxidation)

During annealing, the formed liquid phase L is pushed out of the sheet and aluminum as well as magnesium oxidize simultaneously in air. Oxide nodules started to form on the sheet between 21 and 28 min annealing time at 873 K. Figure 7 shows the top view of the "*Cauliflower*" [6] morphology (1) close to a grain boundary (4) after 56 min. Holes with surrounding deflated areas (5) are observed close to the grain boundary as well. The subjacent shrinkage cavities are formed to compensate the liquid metal displacement. The internal surfaces are oxidized as well, proving reactions with inflowing air, resp. furnace gas. These cavities are apparently caused by metal transport and not by outward diffusion of Mg.

The oxide nodule in Fig. 7 is composed of different oxides, according to EDX analysis, (2) is an AlMgO oxide, rich in MgO with traces of Si, whereas (3) is a mixed oxide with traces of Si, rich in Al_2O_3. Depending on the Mg concentration of the pushed out metal, either an MgO or Al_2O_3 rich oxide is formed first. Amorphous Al_2O_3, MgO and Al_2MgO_4 can form mixed crystals [15] and are defined as mixed oxides in the following. The mixed oxide in reference 6 of Fig. 7 is examined in detail in Fig. 8.

In Fig. 8, the References [7–11] indicate the according EDX point analysis. The analysis in Table 3 shows that the metal matrix (7) is low in Mg and Si, because they were consumed by oxide formation. The composition of the solidified Mg–Si-rich L phase is shown at reference (8). Comparing the initial alloy composition with 4.41 mol % Mg and 0.15 mol% Si, the local concentration of these two elements is more than doubled at this point.

Therefore, annealing at 873 K leads to oxidation of a melt that is highly enriched in Mg and Si. Finally, the mixed oxides (9) and (10) are formed, showing that Si is oxidized as well.

Possible oxide formations from the L1′ and L2′ phase are explained with Fig. 9. This ternary system (Al–Mg–Si) is calculated using the software FactSage with, FactPS, FTlite and FToxide databases [16] at 873 K with 50 mol% oxygen, as it was approximately measured by EDX in the mixed oxide.

The initial alloy composition of the can end sheet is marked with I in Fig. 9. At 873 K, the Mg_2Si phases dissolve in the surrounding α-aluminum and form the liquid

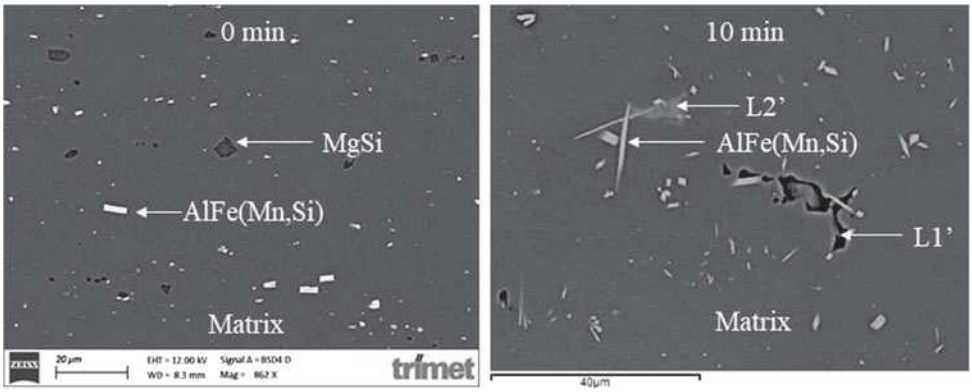

Fig. 6 REM BSE pictures of EN AW-5182 sheet polished cross section before (left) and after isothermal annealing for 10 min at 873 K (right)

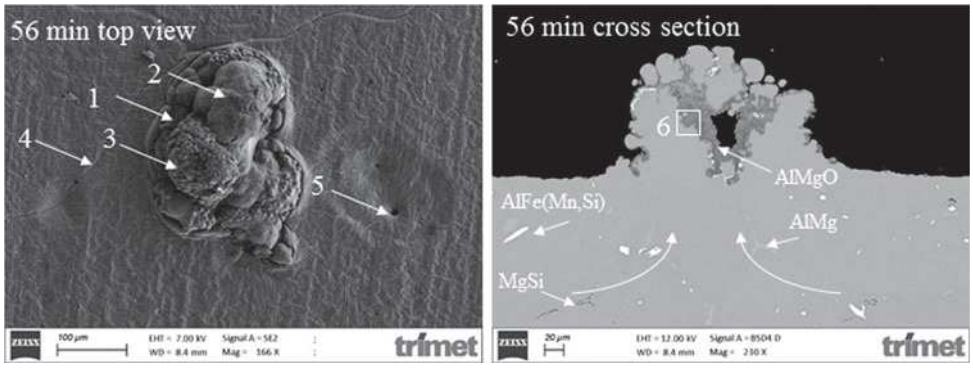

Fig. 7 SEM SE picture of oxide nodule on EN AW-5182 can end sheet after 56 min at 873 K (left) with different oxide phases present (1–3) and cross section of similar structure in SEM BSE mode including proposed mass flow patterns

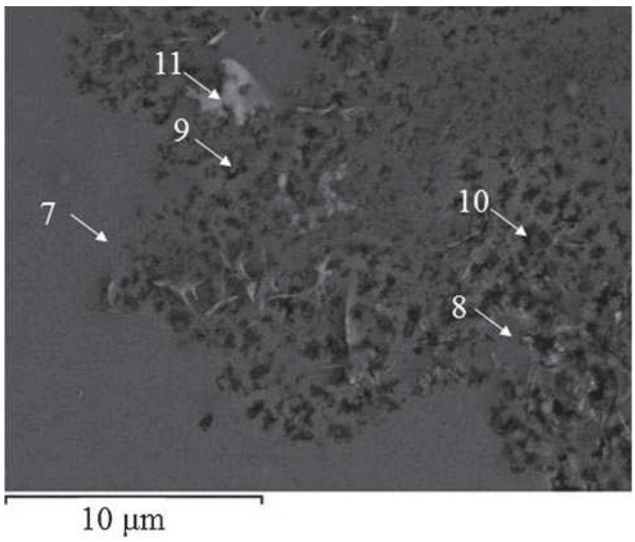

Fig. 8 SEM BSE picture of the oxide nodule morphology at metal matrix and mixed oxides interface

phase L with a composition between L1′ and L2′. The Mg–Si-rich melt L is pushed out of the sheet and oxidizes to the molecular formula of spinel (Al_2MgO_4), which can grow as an amorphous mixture of Al_2O_3 and MgO [15]. It is assumed that the melt is partially trapped in the growing oxide network. As Al and Mg react to their oxides, the local Si concentration increases. With increasing Si concentration, the formation of aluminum silicate $Al[AlSiO_5]$ by direct oxidation becomes thermochemically possible. If silicon is not oxidized directly from melt, Cordierit $Mg_2[AlSi_5O_{18}]$ or AlSi-spinel can be formed by substitution-diffusion or vacancy-diffusion respectively.

If γ-Al_2O_3 is formed, it is defined as a defect spinel and can be written as $\square_8Al_{64}O_{96}$ The eight cation vacancies can be occupied by 8 Si^{4+} anions, whereby the number of Al-ions has to be reduced to maintain charge neutrality. After vacancy diffusion of Si, an AlSi-spinel $2Al_2O_3 \cdot 3SiO_2$ is produced. According to [15], the formation of aluminum silicate and AlSi-spinel lead to cracks and pores in the oxide layer, which promote further metal oxidation. Due to the measured Si concentration <1 mol% in the oxide, it is concluded that Si is present in the form of aluminum silicate or AlSi-spinel. Further investigations could clarify the precise oxide structure.

Deduction of the Oxidation Mechanism and Industry Recommendation

The discussed annealing experiments with EN AW-3104 can body and EN AW-5182 can end sheets show that the thermal pre-treatment temperature of a UBC recycling process has to be limited to 843 K to avoid oxidation of the can end sheet. Above this temperature, first parts of liquid fractions are formed in the can end sheets, while the can body sheets remain completely solid. Formation of the liquid phase leads

Table 3 Quantitative EDX point analysis of [7–11] in Fig. 8

Reference	Phase	Element in mol%				
		Mg	Si	Al	O	C
[7]	Matrix	2.1	0.2	52.8	1.4	42.9
[8]	Mg–Si-rich	14.6	0.3	66.8	17.5	–
[9]	Mixed oxide	34.1	0.4	18.4	46.8	–
[10]	Mixed oxide	31.2	0.8	23.1	44.5	–
[11]	AlFe(Mn, Si)	3.0	0.3	62.6	7.0	–

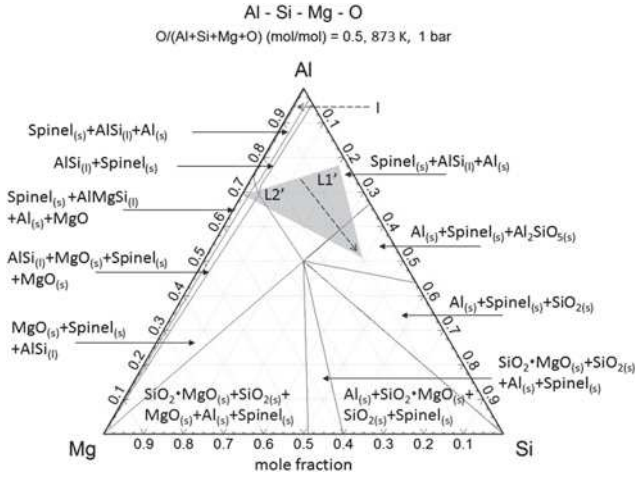

Fig. 9 Ternary phase diagram Al–Mg–Si at 873 K with 50 mol% oxygen in the system calculated using FactSage 7.1 [16] and proposed Si enrichment in the gray area

to molten metal penetration through the protective sheet surface within minutes. This changes the mechanisms from diffusion-controlled oxidation through the MgO layer on the sheet to non-protective liquid metal oxidation. Because the liquid metal is rich in Mg and Si, rapid oxidation and formation of porous oxide nodules is the result. A model for non-protective solid state oxidation of AlMg-alloys with nodular oxide growth was first described by [6]. A new model can now be formulated for liquid metal and gas transport in the semi-solid alloy state. The new model is presented in Fig. 10, where Al_2MgO_4 oxides, rich in Al_2O_3 or MgO are formed on the displaced Mg-Si-rich melt. When the melt is trapped in the oxide nodules, Si can oxidize to aluminum silicate or diffuse into γ-Al_2O_3 forming AlSi-Spinel. Both oxides are non-protective and promote further oxidation.

It is important to note that the can end sheet oxidizes extensively within 10 min, when the metal temperature exceeds 843 K. The formed metal oxides are introduced into the subsequent melting process and increase dross formation by entraining metal into oxide films. For industrial application it is recommended to set the thermal pre-treatment temperature of UBC to 823–843 K. The successful de-coating of UBC requires 823 K pre-treatment temperature and oxygen present in the atmosphere. On the other hand, the temperature has to be limited to 843 K to prevent extensive oxidation of the can end sheets. When other scrap types are processed, the phase-diagrams of according alloys should be checked to choose an applicable process temperature. It is furthermore recommended to use shredded UBC. The increased surface to volume ration allows a faster convective heat transfer and a homogeneous temperature distribution in the material. As a result, the thermal pre-treatment cycle time can be reduced even with a temperature limit of 843 K. Furthermore it is recommended to perform spot sample measurements of the effective scrap temperature during thermal pre-treatment. It has to be ensured that the

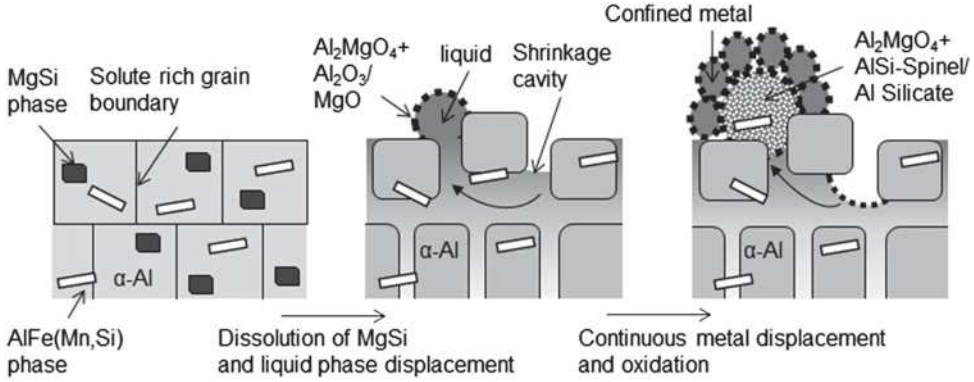

Fig. 10 Model for non-protective oxidation of Al–Mg–Si alloys in semi-solid state at 873 K explaining the three step reaction mechanism (liquid = Mg–Si-rich liquid phase)

temperature limit is not exceeded due to combustion of organic contamination.

Acknowledgements The research leading to these results has been carried out within the framework of the AMAP (Advanced Metals And Processes) research cluster at RWTH Aachen University, Germany.

References

1. A. Kvithyld et al., "Recycling light metals: optimal thermal decoating" *JOM*, 60 (2008), 47–51.
2. A. Escherle, "Application of pyrolysis in aluminium recycling" Erzmetall 55 (2002), 471–478.
3. Christoph Schmitz, *Handbook of Aluminium Recycling*, vol. 2 (Vulkan-Verlag GmbH, Essen, 2014), 33–351.
4. J. Steglich, R. Dittrich, M. Rosefort, B. Friedrich, "Pre-Treatment of Beverage Can Scrap to Increase Recycling Efficiency", *Journal of Materials Science and Engineering* A3 (3–4) (2016), 57–65.
5. S.A. Impey, "The mechanism of dross formation on aluminium and aluminium-magnesium alloys" (Ph.D. thesis, Cranfield University, 1989).
6. M. H. Zayan, "Model for nonprotective oxidation of Al-Mg alloys" *Oxidation of Metals* 34 (1990), 465–472.
7. K. H. Kim, "Formation of endogenous MgO and $MgAl_2O4$ particles and their possibility of acting as substrate for heterogeneous nucleation of aluminum grains" *Surf. Interface Anal.* 47 (4) (2015), 429–438.
8. C. N. Cochran, W. C. Sleppy, "Oxidation of High-Purity Aluminum and 5052 Aluminum-Magnesium Alloy at Elevated Temperatures", *Journal of The Electrochemical Society* 108 (4) (1961), 322–327.
9. D. J. Field, G. M. Scamas, E. P. Butler, "The High Temperature Oxidation of Al-4.2 Wt. Pct. Mg Alloy" *Metallurgical Transactions* 18A (1987), 463.
10. W. Thiele, "Die Oxydation von Aluminium- und Aluminiumlegierungsschmelzen Teil 1" *Aluminium* 38 (11) (1962), 707–715.
11. M. Guermazi, "SiC-reinforced Al2O3/Metal composites by directed metal oxidation" (Ph.D. thesis, McGill University, Montreal, 1996).
12. Pandat™ Version 2017, S. Chen, et al., *CompuTherm LCC*, Madison USA, 2008.
13. Friedrich Ostermann, *Anwendungstechnologie Aluminium*, (Springer-Verlag Berlin Heidelberg, 2014), 171–182.
14. Heinrich Hanemann, Angelica Schrader, *Atlas Metalligraphicus*, (Stahleisen Düsseldorf, 1952), 128–132.
15. Hermann Salmang, Horst Scholze, *Die physikalischen und chemischen Grundlagen der Keramik*, (Springer Verlag, Berlin Heidelberg, 1968), 13–208.
16. FactSage Version 7.1, W. Bale et al., Thermfact Ltd, GTT–Technologies, 2016.